



LAWRENCE
LIVERMORE
NATIONAL
LABORATORY

Modelling of small tungsten dust grains in EAST tokamak with NDS-BOUT++

Z. Liu, R. Ding, X. Q. Xu, N. M. Li

November 30, 2020

Physics of Plasmas

Disclaimer

This document was prepared as an account of work sponsored by an agency of the United States government. Neither the United States government nor Lawrence Livermore National Security, LLC, nor any of their employees makes any warranty, expressed or implied, or assumes any legal liability or responsibility for the accuracy, completeness, or usefulness of any information, apparatus, product, or process disclosed, or represents that its use would not infringe privately owned rights. Reference herein to any specific commercial product, process, or service by trade name, trademark, manufacturer, or otherwise does not necessarily constitute or imply its endorsement, recommendation, or favoring by the United States government or Lawrence Livermore National Security, LLC. The views and opinions of authors expressed herein do not necessarily state or reflect those of the United States government or Lawrence Livermore National Security, LLC, and shall not be used for advertising or product endorsement purposes.

Journal of Nuclear Materials

Modelling of small tungsten dust grains in EAST tokamak with NDS-BOUT++ --Manuscript Draft--

Manuscript Number:	JNUMA-D-21-00587
Article Type:	Full Length Article
Section/Category:	Nuclear fuels and materials
Keywords:	Dust, Tokamak, BOUT++, NDS
Corresponding Author:	Yan Feng, Ph.D. Soochow University Suzhou, CN CHINA
First Author:	Zhuang Liu
Order of Authors:	Zhuang Liu Rui Ding Nami Li Guozhong Deng Jizhong Sun Dezhen Wang Xuexiao Xu Yan Feng, Ph.D.
Abstract:	<p>The Nano Dust Simulation (NDS) module is developed under the BOUT++ framework, a highly desirable C++ code package to perform parallel plasma fluid simulations with an arbitrary number of equations in three-dimensional curvilinear coordinates, to model the transport of small dusts as well as their evolution property along their trajectories. Due to the severe dust ablation in fusion plasmas, the dust size would decrease from micron to nanometer, resulting in impurities. Small dusts in the simulations here are specified as tungsten spheres with the radii on or below the order of submicron. The Rayleigh limit is included in the charging process when the dust is ablated to the droplet phase. The simulation results from the NDS module show that a 200 nm-radius spherical tungsten dust originated from upper divertor region of EAST Tokamak is ablated completely due to the intense heating from the incoming plasma inside the core region, well consistent with the CCD footage of EAST shot # 81459. It is also found that the magnetic field dominates the dust transport when the dust radius is below 100 nm during the ablation along the trajectory. Our simulations also show that a 10 nm-radius spherical tungsten dust injected from the inner midplane is well constrained by the magnetic field and it reaches the inner divertor target with a velocity on the order of km/s.</p>
Suggested Reviewers:	Ahmed Hassanein hassanein@purdue.edu He is knowledgeable about the topic of fusion dusts in Tokamaks. Rajesh Maingi rmaingi@pppl.gov He is knowledgeable about the topic of fusion dusts in Tokamaks. Zhehui Wang zwang@lanl.gov He is knowledgeable about the topic of fusion dusts in Tokamaks.

May 28, 2021

Journal Nuclear Materials

Dear Editor:

We have just submitted our manuscript “Modelling of small tungsten dust grains in EAST tokamak with NDS-BOUT++” to Plasma Physics and Controlled Fusion.

The dust behaviors in tokamaks have been investigated drastically over the past two decades, with a lot of experimental and theoretical discoveries, published quite a few papers on various fusion related journals, such as J. NUCL. MATER., PPCF and NF. However, the transport of small dust grains below the micron size is different from that of larger ones. Here, we incorporate the charging, the ablation and the guiding-center motion of small dust grains into the newly updated NDS-BOUT++. Using this newly updated NDS-BOUT++, we simulate the transport and ablation of dust grains inside the EAST tokamak. We find that our current simulation results are well consistent with the recent dust observation in the EAST tokamak. The consistency indicates that the newly-developed NDS module here is validated by the observed dust in the EAST tokamak experiment.

This study is novel, timely, and important to the fields of fusion plasma physics and tokamak operation. We hope our manuscript can satisfy the publication requirements of Journal Nuclear Materials.

Thank you very much.

Sincerely,

Yan Feng

Professor Yan Feng
Center for Soft Condensed Matter Physics & Interdisciplinary Research,
School of Physical Science and Technology,
No.1 Shi-Zi Street,
Suzhou, Jiangsu, China, 215006
Telephone: +86-512-69156391

Modelling of small tungsten dust grains in EAST tokamak with NDS-BOUT++

Zhuang Liu^{*a}, Rui Ding^b, Nami Li^{c,d}, Guozhong Deng^b, Jizhong Sun^d,
Dezhen Wang^d, Xueqiao Xu^c, Yan Feng^{*a}

^a*Center for Soft Condensed Matter Physics and Interdisciplinary Research, College of Physical Science and Technology, Soochow University, Jiangsu, China*

^b*Institute of Plasma Physics, Chinese Academy of Science, Hefei, China*

^c*Lawrence Livermore National Laboratory, CA, USA*

^d*Physics Department, Dalian University of Technology, Liaoning, China*

Abstract

The Nano Dust Simulation (NDS) module is developed under the BOUT++ framework, a highly desirable C++ code package to perform parallel plasma fluid simulations with an arbitrary number of equations in three-dimensional curvilinear coordinates, to model the transport of small dusts as well as their evolution property along their trajectories. Due to the severe dust ablation in fusion plasmas, the dust size would decrease from micron to nanometer, resulting in impurities. Small dusts in the simulations here are specified as tungsten spheres with the radii on or below the order of submicron. The Rayleigh limit is included in the charging process when the dust is ablated to the droplet phase. The simulation results from the NDS module show that a 200 nm-radius spherical tungsten dust originated from upper divertor region of EAST Tokamak is ablated completely due to the intense heating from the incoming plasma inside the core region, well consistent with the CCD footage of EAST shot # 81459. It is also found that the magnetic field dominates the dust transport when the dust radius is below 100 nm during the ablation along the trajectory. Our simulations also show that a 10 nm-radius spherical tungsten dust injected from the inner midplane is well constrained by the magnetic field and it reaches the inner divertor target with a velocity on the order of km/s.

Keywords: dust, Tokamak, BOUT++, NDS

1
2
3
4
5
6
7
8
9 **1. Introduction**

10
11 Dusts may pose a serious threat to the tokamak operation and safety [1]. It
12 is important to study the behavior of dust grains in tokamaks, which depends
13 heavily on the size and charge of these dusts. Dusts may be radioactive, may
14 contain toxic substances from the vessel wall, may penetrate into the core plasma
15 causing plasma degradation, and sometimes may even result in the termination
16 of the plasma discharges [2]. Some dust granules, such as the lithium or boron
17 pellets, are typically injected into the tokamak plasma intentionally to achieve
18 better H-mode discharges, serving as a help, rather than a hindrance to the
19 tokamak operation [3, 4, 5].

20
21 Due to the excellent thermal endurance and low tritium retention rates [6],
22 tungsten tiles are considered as the primary candidate for plasma-facing com-
23 ponents in the current and future tokamaks. However, during the energetic
24 plasma-wall interactions (PWIs), nano structures, such as fuzz and bubbles,
25 form and introduce massive small dusts into the plasma under the heat load
26 [7, 8, 9, 10]. In addition, small dusts may also be originated from larger mi-
27 crometer to millimeter sized dusts and droplets. In our simulation investigations
28 here, we specify small dusts as spherical dusts with the radius on the order of
29 submicron or blow, to mimic the often generated small dusts in tokamaks. Dur-
30 ing the ablation of small dust grains, considerable amount of impurity is brought
31 into the plasma. The tolerance of tungsten impurity density in the tokamak core
32 region is lower than that of the low-Z impurities [11]. As a result, from the cam-
33 paign in 2017 to that in 2018, the number of disruptions on EAST due to the
34 severe impurity burst has tripled, reaching a high percentage of 38.3% because
35 of the tungsten dust ablation [12]. Furthermore, the H-mode discharge cannot
36 be achieved any more when the impurity density is over one tungsten atom per
37 10^5 hydrogen atoms [13].

38
39 Massive research has been performed to address problems associated with
40 dust charging, ablation, and dynamics in tokamaks. As far as we know, there are
41 mainly five code packages for the tokamak dust simulations, which are DUSTT
42
43
44
45
46
47
48
49
50
51
52
53
54
55
56
57
58
59
60
61
62
63
64
65

1
2
3
4
5
6
7
8
9 [14], DTOKS [15], MIGRAINE [16], DUSTTRACK [17] and DUMBO [18], re-
10 spectively. From our literature search, we find that the existing tokamak dust
11 transport code packages mainly simulate the dust grains with the radii larger
12 than $1 \mu\text{m}$, in which case, the drift effect due to the electromagnetic field can
13 be reasonably ignored. However, for smaller dusts, the drift effect may become
14 a dominant factor, so that a new model system based on the guiding-center
15 motion needs to be established. Instead of the gravity and the ion drag force
16 for larger dusts, the transport of small dusts is mainly dominated by both the
17 Lorentz force and the ion drag force as in [19], where the Larmor radius for the
18 small dust in the typical tokamak fusion environment is also assessed.
19

20
21
22
23
24
25 In this work, we present the Hamiltonian guiding center transport model for
26 small dust grains, and compare our simulation results with the CCD footage of
27 dusts in the EAST tokamak experiment. Based on the well-known Hamiltonian
28 guiding center equation of motion by Littlejohn et al. [20], the NDS-BOUT++
29 is introduced in the 3D coordinate system in the realistic tokamak flux surface
30 and divertor geometry [21]. Using the newly updated NDS-BOUT++ code
31 package, the trajectories and velocities of dust grains with different sizes can be
32 obtained, so that an operation approach to prevent the dust contamination to
33 the core plasma and optimize the tokamak vessel wall can be achieved.
34
35
36
37
38

39 This paper is organized as follows. The NDS model is presented in Section
40 2, including the three subsections of dust charging, dust ablation, and dust
41 transport. In Section 3, we describe our simulations performed under the real
42 EAST geometry. In Section 3.1, our simulation result of the dust trajectory
43 originated from the upper divertor region is compared with the CCD footage
44 of the EAST tokamak discharge. In Section 3.2, we also report our simulations
45 to study the dust grain launched from the midplane. Finally, it is our brief
46 summary in Section 4.
47
48
49
50
51
52
53
54
55
56
57
58

1
2
3
4
5
6
7
8
9 **2. Model**

10
11 *2.1. Dust charging*

12
13 The equilibrium floating potential of dusts immersed in plasmas can be ob-
14 tained by solving the current balance on the dust grain. The main charging
15 mechanisms on dusts in tokamaks include the collection of the plasma ions and
16 electrons, the secondary electron emission (SEE) and the thermionic electron
17 emission (TEE) from the dust surface [22]. The orbital motion limited (OML)
18 theory [23] is employed to describe the plasma ion and electron currents, noted
19 as I_i and I_e , respectively. The bombardment between the energetic incoming
20 plasma electrons and the dust grains results in the SEE. To improve the ac-
21 curacy while dealing with the SEE yield, we use the Young–Dekker formula to
22 replace the Sternglass formula in the NDS model, similar to [24]. For tungsten
23 dusts, the SEE yield may exceed the absorbed electrons, which means $\delta_{SEE} > 1$
24 when the plasma temperature is on the order of several hundred eV. In such
25 plasma environment, the TEE also occurs and may become a dominate factor
26 while the dust temperature increases. The Richardson-Dushman equation pro-
27 vides a detailed description of the TEE [25]. The overall dust charging equation
28 is expressed as
29
30
31
32
33
34
35
36
37
38
39

40
41
$$\frac{dQ}{dt} = \sum I = I_i + I_e + I_{SEE} + I_{TEE}, \quad (1)$$

42

43 where Q is the equilibrium dust charge. When dusts are ablated to the droplet
44 phase, they will undergo the total electrostatic breakup if their charge ex-
45 ceeds the well-known Rayleigh limit [26], which imposes a minimum size on
46 the droplets. The Rayleigh limit is given by
47
48
49

50
51
$$Q = 8\pi(\epsilon_0\gamma R_d^3)^{1/2}, \quad (2)$$

52

53 where ϵ_0 , γ and R_d are the vacuum dielectric constant, the surface tension of the
54 liquid, and the ablated dust radius, respectively. By comparing the dust OML
55 charge to the Rayleigh limit, we find that, in tokamak conditions, the influences
56
57
58

of the electrostatic disintegration on dust charging process is important. The detailed results and the corresponding discussions are presented in Section 3.

2.2. Dust ablation

We include five heating and cooling mechanisms in our dust ablation model, which are the particle bombardment, the electron emission, the recombination processes, the neutral particle emission, and the radiative cooling, respectively. The net power flux deposited on the dust surface is [27]

$$\Xi_{net} = \Xi_i + \Xi_e - \Xi_{SEE} - \Xi_{TEE} + \Xi_{Rec} - \Xi_{Neu} - \Xi_{Rad}. \quad (3)$$

The collection of plasma ions and electrons, $\Xi_i + \Xi_e$, is included in the particle bombardment section, where the fraction of energy backscattered \bar{R}_E is obtained based on an empirical fit to the experimental data of [28]. The power flux of the electron emission mechanism Ξ_{SEE} and Ξ_{TEE} are described by the Young–Dekker formula and the Richardson–Dushman equation, respectively, as mentioned above. Here, Ξ_{Rec} is described as the liberated energy after the recombination of electrons and ions. For hydrogen atoms, the energy per reaction is 13.6 eV [27]. We assume that all ions incident on the grain would recombine with electrons, due to the number of free electrons loosely bound to the surface for the case of negative equilibrium potential of dusts. For the positively charged dusts, the backscattered ions do not contribute. The fraction of the backscattered ions is obtained by integrating over the ion distribution. Finally, Ξ_{Rad} represents the radiative cooling power flux which is dictated by the Stefan’s law [27].

The dust temperature T_d is then derived from the heating equation

$$\frac{m_d c(T_d) dT_d}{dt} = 4\pi R_d^2 \Xi_{net}, \quad (4)$$

where m_d and $c(T_d)$ are the dust mass and heat capacity, respectively. The phase transition occurs when the dust temperature reaches the melting, vaporizing, or sublimation points. The size and mass of dust start decreasing once the amount

of the absorbed energy satisfies the dust latent heat h . The radius and mass evolution of dusts are described as follows

$$\frac{dR_d}{dt} = \frac{\Xi_{net}}{\rho h}, \quad (5)$$

$$\frac{dm_d}{dt} = \frac{4\pi R_d^2 \Xi_{net}}{h}. \quad (6)$$

2.3. Dust transport

In this work, the Hamiltonian guiding center equation of motion is used to compare to the helical motion of the tungsten dust on the CCD footage of EAST shot #81459. The Hamiltonian guiding center equations of motion are [27]

$$\frac{d\mathbf{X}}{dt} = \frac{1}{1 + \rho_{\parallel} \mathbf{B} \cdot \nabla \times \mathbf{B}/B^2} \left[q\rho_{\parallel} \mathbf{B}/m_d + (q\rho_{\parallel}^2/m_d) \nabla \times \mathbf{B} + \mathbf{B} \times \nabla H/qB^2 \right], \quad (7)$$

$$\frac{d\rho_{\parallel}}{dt} = -\frac{1}{qB^2(1 + \rho_{\parallel} \mathbf{B} \cdot \nabla \times \mathbf{B}/B^2)} \left[\nabla H \cdot \mathbf{B} + \rho_{\parallel} \nabla H \cdot \nabla \times \mathbf{B} \right] + \pi R_d^2 m_d m_p N_i |V_p - V_d| (V_p - V_d), \quad (8)$$

where X is the guiding-center position of the particle and $\rho_{\parallel} = mv_{\parallel}/qB$ is the parallel Larmor radius. The Hamiltonian H has the form of

$$H(\mathbf{X}, \rho_{\parallel}) = (q^2/2m_d)\rho_{\parallel}^2 B^2 + \mu B + q\Phi + m_d g Z. \quad (9)$$

The last two terms in the Hamiltonian represent the influences from the electric field and the gravity, respectively.

3. Results and Discussion

3.1. Dust injected from upper divertor

As the chief result of this paper, we compare our NDS-BOUT++ modeling with the recent experiment shot # 81459 on the EAST tokamak. In the shot #

81459 of the EAST tokamak, a large number of dusts and droplets are generated from the upper divertor region, causing the final disruption when they enter the core plasma during the discharge. Figure 1 shows the CCD footage of a dust originates from upper divertor region, which transports in the form of the helical trajectory. To study the helical trajectory of the dust in this case, a guiding-center motion description of dusts is provided in the steady state plasma conditions, reconstructed with the BOUT++ transport module based on the experiment measurements. The corresponding plasma density, temperature, potential, and ion parallel velocity profiles are obtained, as presented in Fig. 2.

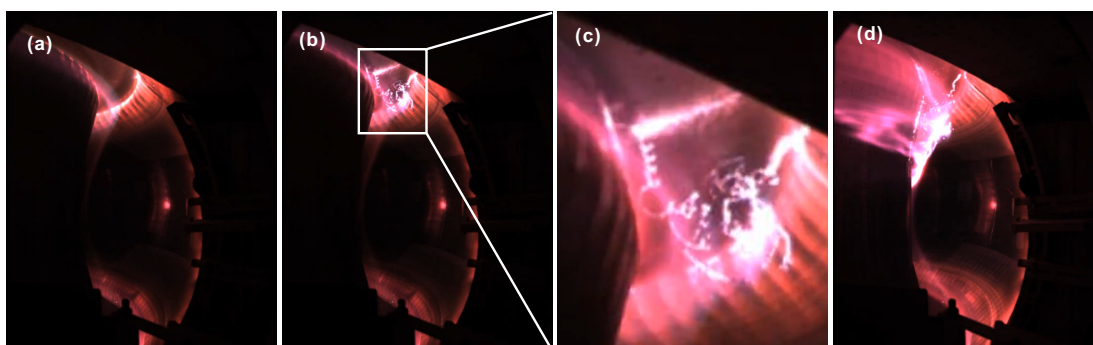


Figure 1: Images captured by a CCD camera mounted on the midplane of EAST for the discharge #81459 of (a) H - mode discharge when $t = 3.700\text{s}$ without the substantial dust generation, (b) when $t = 3.827\text{s}$, large amounts of dusts generated during PWIs and some transport in the form of guiding-center motion, and (c) a magnified view of the divertor region at this moment, as well as (d) when $t = 3.836\text{s}$, the formation and transport of dusts (or droplets) cause the final disruption

Since it is not feasible to directly determine the initial dust radius only from this CCD footage, we estimate the dust radius from the Larmor radius of the dust trajectory. Based on the plasma and the magnetic field profiles in the EAST upper divertor region, the initial tungsten dust radius and velocity along the magnetic field is specified as 200 nm and 100 m/s, respectively. The modelling of the dust formation during the PWIs may provide the initial dust profiles with a higher precision, which is well beyond the scope of the current paper.

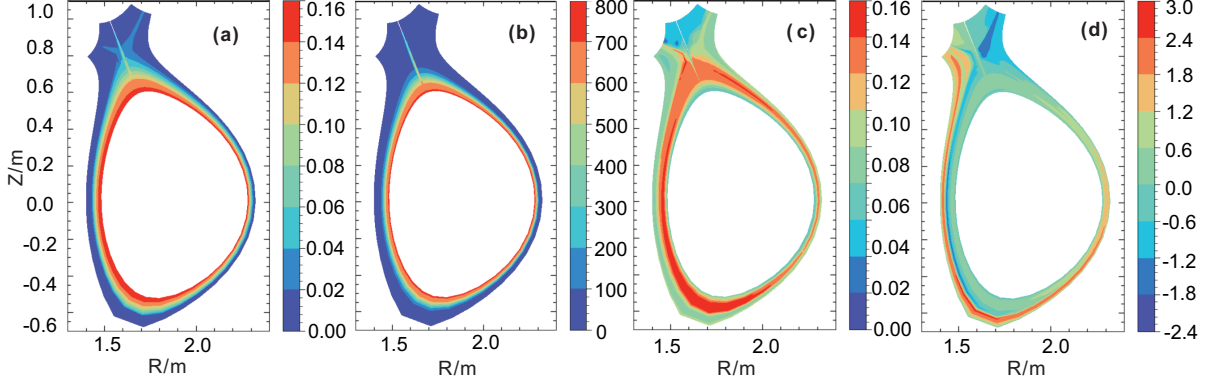


Figure 2: The obtained (a) electron temperature in $10^{20}m^{-3}$, (b) electron density in eV , (c) plasma potential in V , and (d) ion parallel velocity profiles in $10^5m/s$ from the reconstructed EAST upper singlenull background plasma using the BOUT++ transport module.

Our obtained dust guiding-center trajectory modelled with the NDS-BOUT++ is presented in Fig. 3(a), and further magnified in (b) using the solid curve. The region encircled by the long-dashed line is the BOUT++ simulation domain, while the short-dashed black line represents the Separatrix.

It can be seen that the dust launched from the upper divertor region heads directly for the core plasma. This dust is finally ablated completely at the position around $R = 1.51$ m, $Z = 0.49$ m. Our obtained guiding-center trajectory in Fig. 3 is in good agreement with the experiment CCD footage in Fig. 1. In the experiment, the final stage of the helical motion seems to experience a sudden increase of the Larmor radius, followed by a reverse of the gyro direction. We speculate that this might be caused by unexpected collisions.

From the obtained dust guiding-center trajectory in Fig. 3, it clear that the magnetic field does not dominate the dust motion before the dust enters the core region. The simulated dust crosses multiple magnetic surfaces including the Separatrix under the combined effects of the Lorentz force, the gravity and the ion drag force. The dust charge-to-mass ratio can be expressed as

$$\frac{Q}{m_d} = \frac{4\pi\epsilon_0 R_d \phi_s}{4\pi R_d^3/3} = \frac{3\epsilon_0 V_{ds} k_B T_e}{R_d^2 \rho_e}, \quad (10)$$

where ϕ_s is the dust surface potential and V_{ds} is the normalized dust equilibrium potential. The charge-to-mass ratio is inversely proportional to R_d^2 , which means that the electromagnetic field dominates the dust transport when its size is decreased to a critical value during the ablation. At the end of the trajectory starting from $Z = 0.53$ m, marked with the arrow in Fig. 3(b), the guiding center trajectory clearly starts to turn parallel to the magnetic field lines, probably due to the fact that the the Lorentz force gradually dominates the dust motion while the dust size decreases when it ablates.

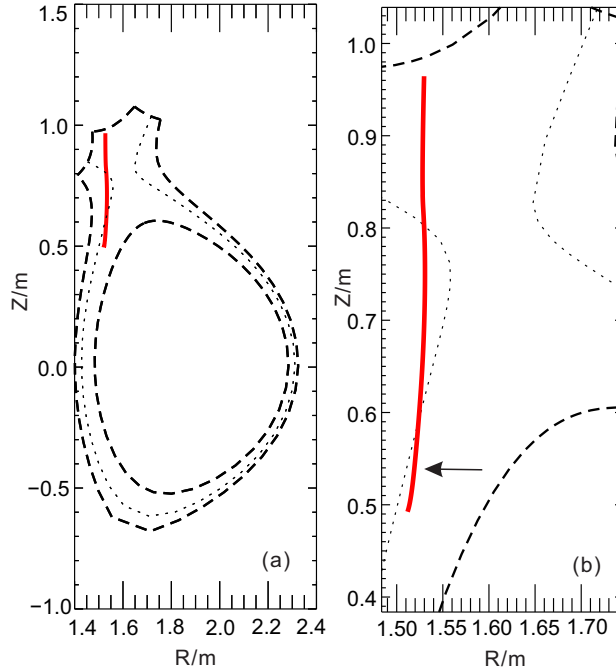


Figure 3: The obtained guiding-center trajectory (represented by the red full line) of the 200 nm-radius spherical tungsten dust injected from divertor region of EAST tokamak using the NDS-BOUT+ modeling (a) and the corresponding magnified view (b). This trajectory from our simulations is well consistent with the CCD footage captured during the experiment of EAST shot # 81459. The trajectory begins turning parallel to the magnetic field after the dust crosses the Separatrix and enters the core region.

To study the critical value of dust radius when the the Lorentz force becomes the dominating effect on the dust motion during its transport, the evolution of

1
2
3
4
5
6
7
8
9
10
11
12
13
14
15
16
17
18
19
20
21
22
23
24
25
26
27
28
29
30
31
32
33
34
35
36
37
38
39
40
41
42
43
44
45
46
47
48
49
50
51
52
53
54
55
56
57
58
59
60
61
62
63
64
65

the dust radius and the dust position on the Z axis along the trajectory are presented in Fig. 4. In Fig. 4, the radius values and the Z coordinates are represented by the solid and dashed curves, respectively. It can be seen that the total transport time is 3.9 ms. When the time is around 2.5 ms, the dust size begins decreasing due to the ablation. The corresponding Z coordinate at 2.5 ms is around 0.6 m. From Fig. 3, this happens when the dust just crosses the Separatrix and heads for the core region.

The guiding-center trajectory has an obvious turning parallel to the magnetic field starting from the position of $Z = 0.53$ m in Fig. 3. From Fig. 4, it can be seen that the corresponding time is at around 3.5 ms and the dust radius then is around 100 nm. Thus, it seems that it can be concluded that, for the EAST upper single-null discharge, the critical radius of the tungsten dust for the transport transition is around 100 nm.

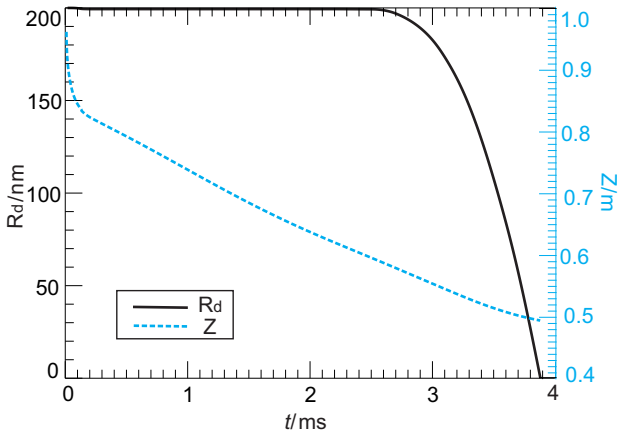
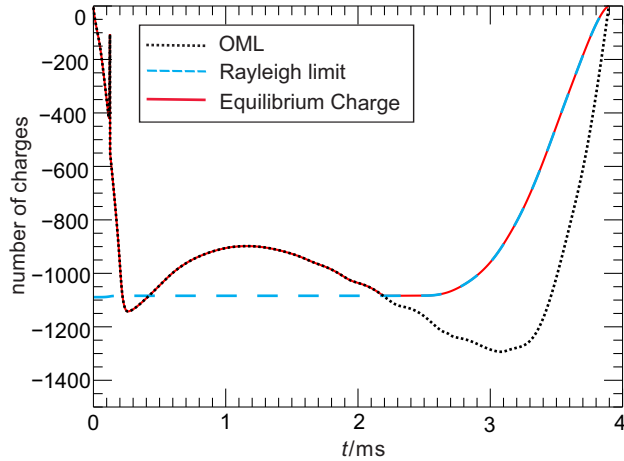


Figure 4: The evolution of the radius of our simulated dust and its trajectory along the Z axis. The ablation becomes severe starting from $t = 2.5$ ms. The Z coordinate then is around 0.6m where the dust crosses the Separatrix.

Here, we provide our determined charge on the dust including the Rayleigh limit, as compared with the widely used OML theory. The Rayleigh limit charge and the dust charge from the OML theory are presented together with the dust equilibrium charge along the dust trajectory in Fig. 5. It can be seen that the

1
 2
 3
 4
 5
 6
 7
 8
 9 OML charge exceeds the Rayleigh limit after around 2.3 ms, just before the
 10 substantial decrease of the dust radius due to the ablation starting at 2.5 ms.
 11 In this case, the dust experiences the electrostatic breakup so that the charges
 12 on the dust are ejected until the Rayleigh limit is satisfied [26]. As a result,
 13 the equilibrium charge on the dust is governed by the Rayleigh limit during the
 14 droplet phase.
 15
 16
 17
 18



19
 20
 21
 22
 23
 24
 25
 26
 27
 28
 29
 30
 31
 32
 33
 34
 35 Figure 5: The time series of the OML charge and the Rayleigh limit charge while the dust
 36 travels in the tokamak. When $t > 2.3$ ms, the OML charge exceeds the Rayleigh limit, as a
 37 result, the dust charges are ejected until the Rayleigh limit is satisfied then.
 38
 39
 40

41 3.2. Dust injected from midplane

42
 43 Dusts are usually generated where the PWI are severe, such as divertor and
 44 midplane regions. In the current simulation, we assume a dust generated from
 45 the midplane. As the second result in this paper, we predict the transport of
 46 a tungsten dust with a much smaller radius in the EAST tokamak using the
 47 validated NDS module. In our simulation with the NDS module, we specify the
 48 simulated tungsten dust as a 10 nm-radius tungsten sphere, launched from the
 49 midplane on the high field side with an initial velocity of 100 m/s along the
 50 magnetic field. Our obtained trajectory is presented in Fig. 6(a) and magnified
 51 in Fig. 6(b).
 52
 53
 54
 55
 56
 57
 58
 59
 60
 61
 62
 63
 64
 65

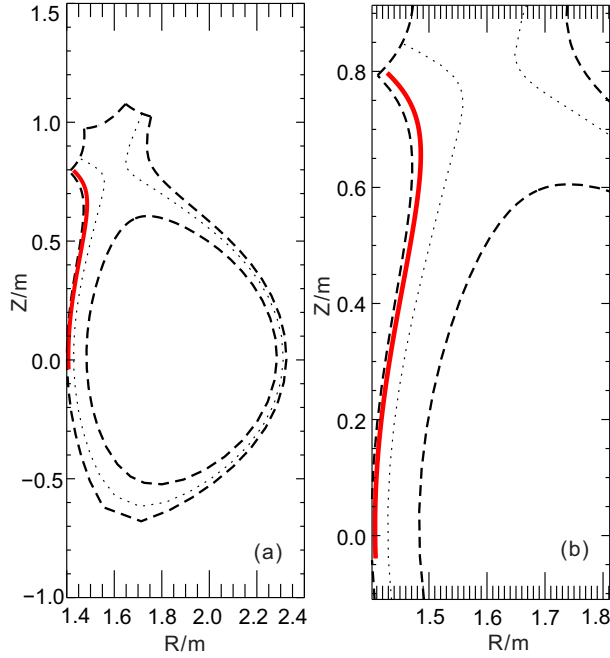


Figure 6: The obtained guiding-center trajectory of a 10nm-radius spherical tungsten dust injected from the EAST inner midplane region using the NDS-BOUT+ modeling (a) and the corresponding magnified view (b). The dust is well constrained by the magnetic field, which transports along the magnetic field, and finally reaches the divertor target.

From Fig. 6, clearly the simulated dust grain is completely constrained by the magnetic field, which transports along the magnetic surface towards the inner upper divertor. Since the trajectory is on the edge outside the Separatrix, where the background plasma profile is relatively mild, the ablation process is subtle so that the dust radius remains almost unchanged during the entire transport.

Due to the acceleration by the ion drag force, the simulated dust reaches the divertor plate with a parallel velocity of around 2.8 km/s. Our obtained parallel velocities along the trajectory for both the dust and the ion are presented in Fig. 7, represented by the solid and dashed curves, respectively. From the previous study with LS-DYNA [29], the dust transports with the velocity on the order of km/s may result in damages on the divertor plate, thus these damages

1
2
3
4
5
6
7
8
9
10
11
12
13
14
15
16
17
18
19
20
21
22
23
24
25
26
27
28
29
30
31
32
33
34
35
36
37
38
39
40
41
42
43
44
45
46
47
48
49
50
51
52
53
54
55
56
57
58
59
60
61
62
63
64
65

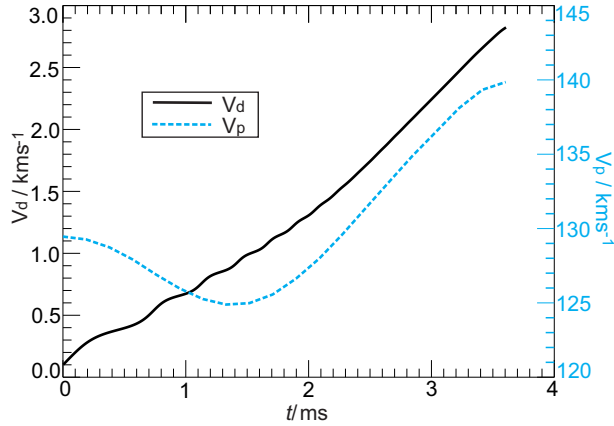


Figure 7: The obtained parallel velocities of our simulated dust of 10 nm-radius and the ion velocity along the trajectory. From our simulations, the dust reaches the divertor with the velocity on the order of km/s due to the ion drag effect of the plasma.

potentially bring more dusts into the tokamak, which transport similarly to the results in section 3.1.

4. Summary

In summary, we develop the NDS module under the BOUT++ framework to study the charging, ablation, and transport of dusts in the real tokamak geometry. The Rayleigh limit is included in the charging process when the dust is ablated to the droplet phase. The guiding-center orbits of tungsten dusts are tracked and compared with the existing dust related experiments on the EAST tokamak. From our simulations, the dust injected from upper divertor is ablated completely after crossing the Separatrix. In this case, the Lorentz force begins dominating the dust transport when the dust radius is below 100 nm during the ablation along the trajectory. A 10 nm-radius tungsten dust launched from the midplane with an initial velocity along the magnetic field is well constrained, which reaches the divertor plate with the velocity on the order of km/s. The dust with this high speed strikes on the divertor plates may cause damages, resulting in further generation of dust particles.

1
2
3
4
5
6
7
8
9 **Acknowledgments**

10
11 This work was supported by National MCF Energy R& D Program of China
12 No. 2018YFE0310100 and the corresponding Supporting Project from the
13 Suzhou Science and Technology Bureau, and also under the auspices of U.S.
14 Department of Energy by Lawrence Livermore National Laboratory under Con-
15 tract No. DE-AC52-07NA27344 LLNL-JRNL-817197.
16
17
18
19

20
21 **References**

- 22
23 [1] J. P. Sharpe, D. A. Petti, H. W. Bartels, A review of dust in fusion devices:
24 Implications for safety and operational performance, Fusion Engineering
25 and Design 63-64 (2002) 153–163.
26
27
28 [2] S. I. Krasheninnikov, R. D. Smirnov, D. L. Rudakov, Dust in magnetic
29 fusion devices, Plasma Physics and Controlled Fusion 53 (8) (2011) 083001.
30
31
32 [3] L. R. Baylor, N. Commaux, T. C. Jernigan, S. J. Meitner, S. K. Combs,
33 R. C. Isler, E. A. Unterberg, T. E. Brooks, N. H. and Evans, A. W. Leonard,
34 T. H. Osborne, P. B. Parks, P. B. Snyder, E. J. Strait, M. E. Fenstermacher,
35 C. J. Lasnier, R. A. Moyer, A. Loarte, G. T. A. Huijsmans, S. Futatani,
36 Reduction of edge localized mode intensity on dIII-d by on-demand trigger-
37 ing with high frequency pellet injection and implications for iter, Physics
38 of Plasmas 20 (8) (2013) 082513.
39
40
41 [4] F. Gao, J. Z. Sun, Z. Sun, G. Z. Zuo, J. S. Hu, A. Loarte, X. Bonnin,
42 L. Peng, J. Y. Liu, Numerical simulation of li-pellet injection experiments
43 for elm-pacing in east, Nuclear Fusion 60 (6) (2020) 066022.
44
45
46 [5] R. Maingi, J. S. Hu, Z. Sun, A. Diallo, K. Tritz, Y. Z. Qian, W. Xu, G. Z.
47 Zuo, C. L. Li, M. Huang, Y. Ye, A. Bortolon, E. P. Gilson, R. Lunsford,
48 D. K. Mansfield, A. Nagy, J. P. Qian, X. Z. Gong, Elm suppression by
49 boron powder injection and comparison with lithium powder injection on
50 east, Journal of Fusion Energy 39 (6) (2020) 429–435.
51
52
53
54
55
56
57
58

- 1
2
3
4
5
6
7
8
9 [6] Y. Xu, J. Wang, H. Zhou, F. Liu, Z. Li, X. C. Li, T. Lu, H. D. Liu, F. Ding,
10 H. M. Mao, M. Z. Zhao, C. G. Lin, G. N. Luo, Plasma exposure behavior
11 of re-deposited tungsten on structural materials of fusion reactors, *Journal*
12 *of Nuclear Materials* 488 (2017) 129–133.
13
14
15
16 [7] Y. Ueda, K. Miyata, Y. Ohtsuka, H. T. Lee, M. Fukumoto, S. Brezin-
17 sek, J. W. Coenen, A. Kreter, A. Litnovsky, V. Philipps, B. Schweer,
18 G. Sergienko, T. Hirai, A. Taguchi, Y. Torikai, K. Sugiyama, T. Tan-
19 abe, S. Kajita, N. Ohno, T. Team, Exposure of tungsten nano-structure to
20 textor edge plasma, *Journal of Nuclear Materials* 415 (1) (2011) S92–S95.
21
22
23
24 [8] P. McCarthy, D. Hwangbo, M. Bilton, S. Kajita, J. W. Bradley, Enhanced
25 fuzzy tungsten growth in the presence of tungsten deposition, *Nuclear Fu-*
26 *sion* 60 (2) (2020) 026012.
27
28
29
30 [9] S. I. Krasheninnikov, Viscoelastic model of tungsten 'fuzz' growth, *Physica*
31 *Scripta* T145 (2011) 014040.
32
33
34 [10] S. I. Krasheninnikov, R. D. Smirnov, On bubbly structures in plasma facing
35 components, *Journal of Nuclear Materials* 438 (2013) S861–S864.
36
37
38 [11] S. Peillon, G. Dogniaux, M. Payet, E. Bernard, G. Pieters, S. Feuillas-
39 tre, S. Garcia-Argote, F. Gensdarmes, C. Arnas, F. Miserque, N. Herlin-
40 Boime, C. Grisolia, O. Pluchery, Dust sampling in west and tritium reten-
41 tion in tokamak-relevant tungsten particles, *Nuclear Materials and Energy*
42 24 (2020) 100781.
43
44
45
46 [12] B. F. Gao, R. Ding, H. Xie, L. Zeng, L. Zhang, B. G. Wang, C. J. Li, D. H.
47 Zhu, R. Yan, J. L. Chen, Plasma-facing components damage and its effects
48 on plasma performance in east tokamak, *Fusion Engineering and Design*
49 156 (2020) 111616.
50
51
52
53 [13] J. W. Coenen, B. Bazylev, S. Brezinsek, V. Philipps, T. Hirai, A. Kreter,
54 J. Linke, G. Sergienko, A. Pospieszczyk, T. Tanabe, Y. Ueda, U. Samm,
55 T. Team, Tungsten melt layer motion and splashing on castellated tungsten
56
57
58

1
2
3
4
5
6
7
8
9 surfaces at the tokamak textor, *Journal of Nuclear Materials* 415 (2011)
10 S78–S82.

11
12 [14] R. D. Smirnov, S. I. Krasheninnikov, Time-dependent modeling of dust
13 outburst into tokamak divertor plasma, *Physics of Plasmas* 27 (8) (2020)
14 082509.
15
16

17
18 [15] M. Bacharis, M. Coppins, J. E. Allen, Dust in tokamaks: An overview of
19 the physical model of the dust in tokamaks code, *Physics of Plasmas* 17 (4)
20 (2010) 042505.
21
22

23 [16] L. Vignitchouk, S. Ratynskaia, P. Tolias, R. A. Pitts, G. De Temmerman,
24 M. Lehnen, D. Kiramov, Survival and in-vessel redistribution of beryllium
25 droplets after iter disruptions, *Nuclear Fusion* 58 (7) (2018) 076008.
26
27

28 [17] A. Uccello, G. Gervasini, F. Ghezzi, E. Lazzaro, D. Borodin, I. Borodkina,
29 D. Douai, A. Huber, I. Jepu, D. Terranova, A. Widdowson, J. Contribu-
30 tors, An insight on beryllium dust sources in the jet iter-like wall based on
31 numerical simulations, *Plasma Physics and Controlled Fusion* 62 (6) (2020)
32 064001.
33
34
35
36

37 [18] A. Autricque, S. H. Hong, N. Fedorczak, S. H. Son, H. Y. Lee, I. Song,
38 W. Choe, C. Grisolia, Simulation of w dust transport in the kstar tokamak,
39 comparison with fast camera data, *Nuclear Materials and Energy* 12 (2017)
40 599–604.
41
42
43

44 [19] S. I. Krasheninnikov, T. K. Soboleva, D. A. Mendis, Dynamics of nano-
45 dust in tokamak edge plasma, *Journal of Nuclear Materials* 415 (1) (2011)
46 S1111–S1114.
47
48

49 [20] R. G. Littlejohn, Variational principles of guiding centre motion, *Journal*
50 *of Plasma Physics* 29 (1983) 111–125.
51
52

53 [21] B. D. Dudson, M. V. Umansky, X. Q. Xu, P. B. Snyder, H. R. Wilson,
54 Bout++: A framework for parallel plasma fluid simulations, *Computer*
55 *Physics Communications* 180 (9) (2009) 1467–1480.
56
57
58

- 1
2
3
4
5
6
7
8
9 [22] Z. Liu, D. Z. Wang, G. Miloshevsky, Simulation of dust grain charging
10 under tokamak plasma conditions, *Nuclear Materials and Energy* 12 (2017)
11 530–535.
12
13
14 [23] G. L. Delzanno, X. Z. Tan, Comparison of dust charging between orbital-
15 motion-limited theory and particle-in-cell simulations, *Physics of Plasmas*
16 22 (11) (2015) 113703.
17
18
19 [24] P. Toliás, On secondary electron emission and its semi-empirical descrip-
20 tion, *Plasma Physics and Controlled Fusion* 56 (12) (2014) 123002.
21
22
23 [25] A. Autricque, S. A. Khrapak, L. Couedel, N. Fedorczak, C. Arnas, J. M.
24 Layet, C. Grisolia, Electron collection and thermionic emission from a
25 spherical dust grain in the space-charge limited regime, *Physics of Plas-
26 mas* 25 (6) (2018) 063701.
27
28
29 [26] M. Coppins, Electrostatic breakup in a misty plasma, *Physical Review*
30 *Letters* 104 (6) (2010) 065003.
31
32
33 [27] Z. Liu, X. T. Xiao, X. Q. Xu, N. M. Li, T. F. Tang, D. Z. Wang, Modelling of
34 nanometer scale dust grains in tokamak, *Contributions to Plasma Physics*
35 60 (5-6) (2020) e201900136.
36
37
38 [28] E. W. Thomas, R. K. Janev, J. Smith, Scaling of particle reflection co-
39 efficients, *Nuclear Instruments and Methods in Physics Research Section*
40 *B-Beam Interactions with Materials and Atoms* 69 (4) (1992) 427–436.
41
42
43 [29] R. D. Smirnov, S. I. Krasheninnikov, A. Y. Pigarov, D. J. Benson,
44 M. Rosenberg, D. A. Mendis, Modeling of velocity distributions of dust
45 in tokamak edge plasmas and dust-wall collisions, *Journal of Nuclear Ma-
46 terials* 390-91 (2009) 84–87.
47
48
49
50
51
52
53
54
55
56
57
58
59
60
61
62
63
64
65

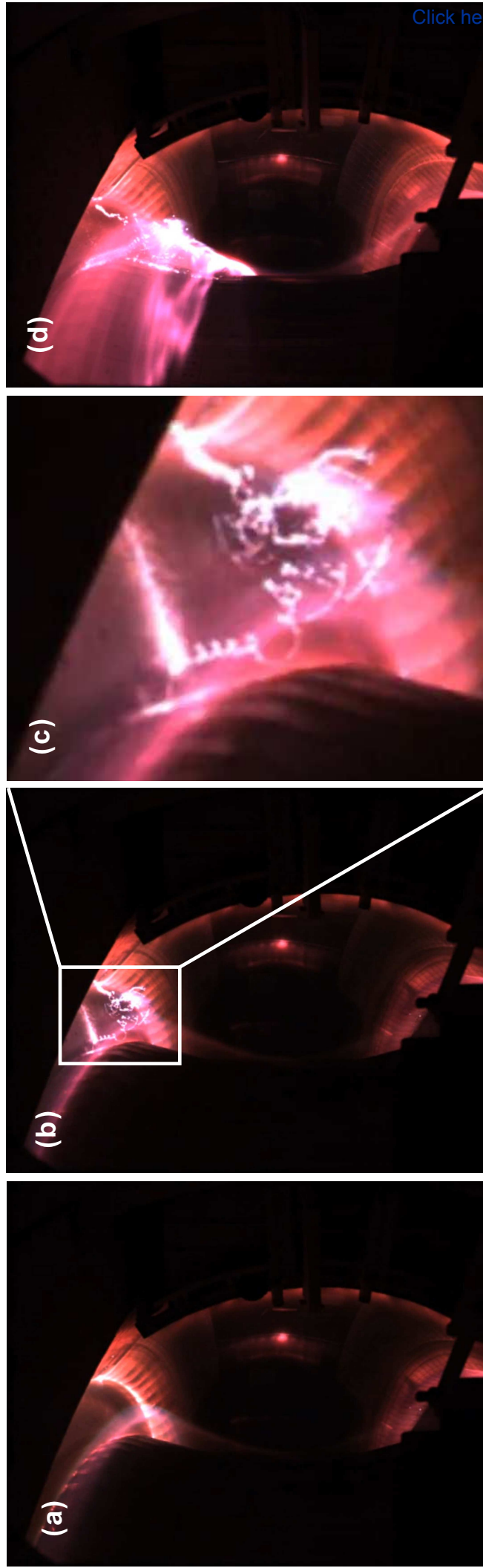
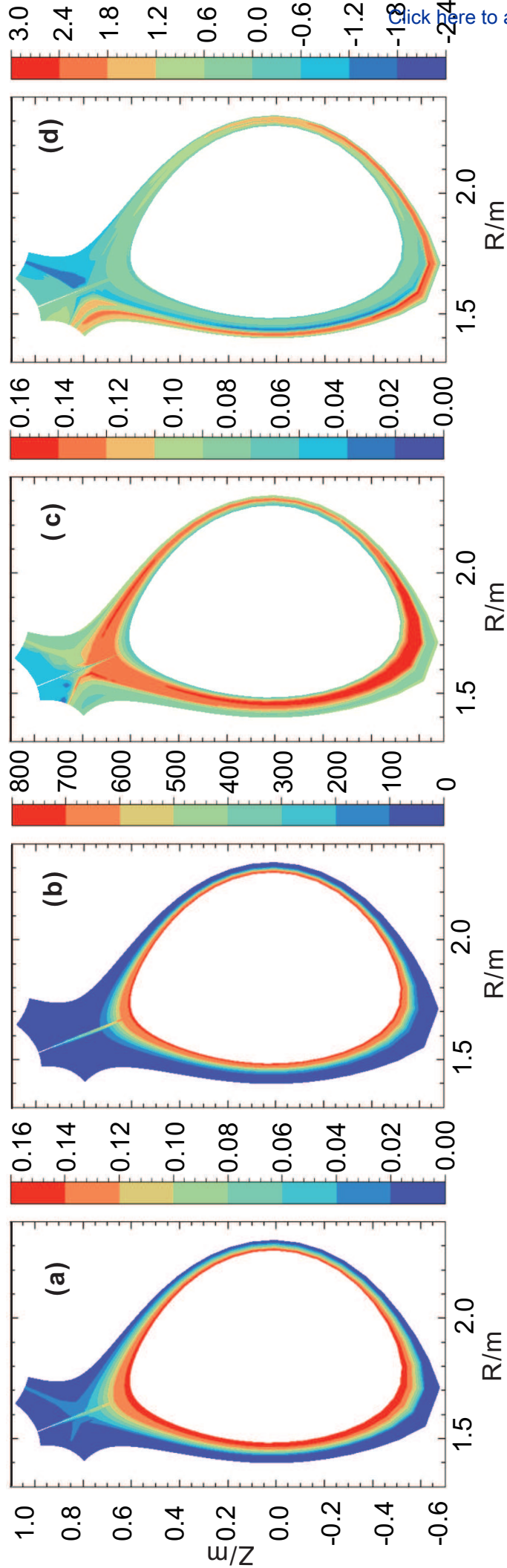


Fig2



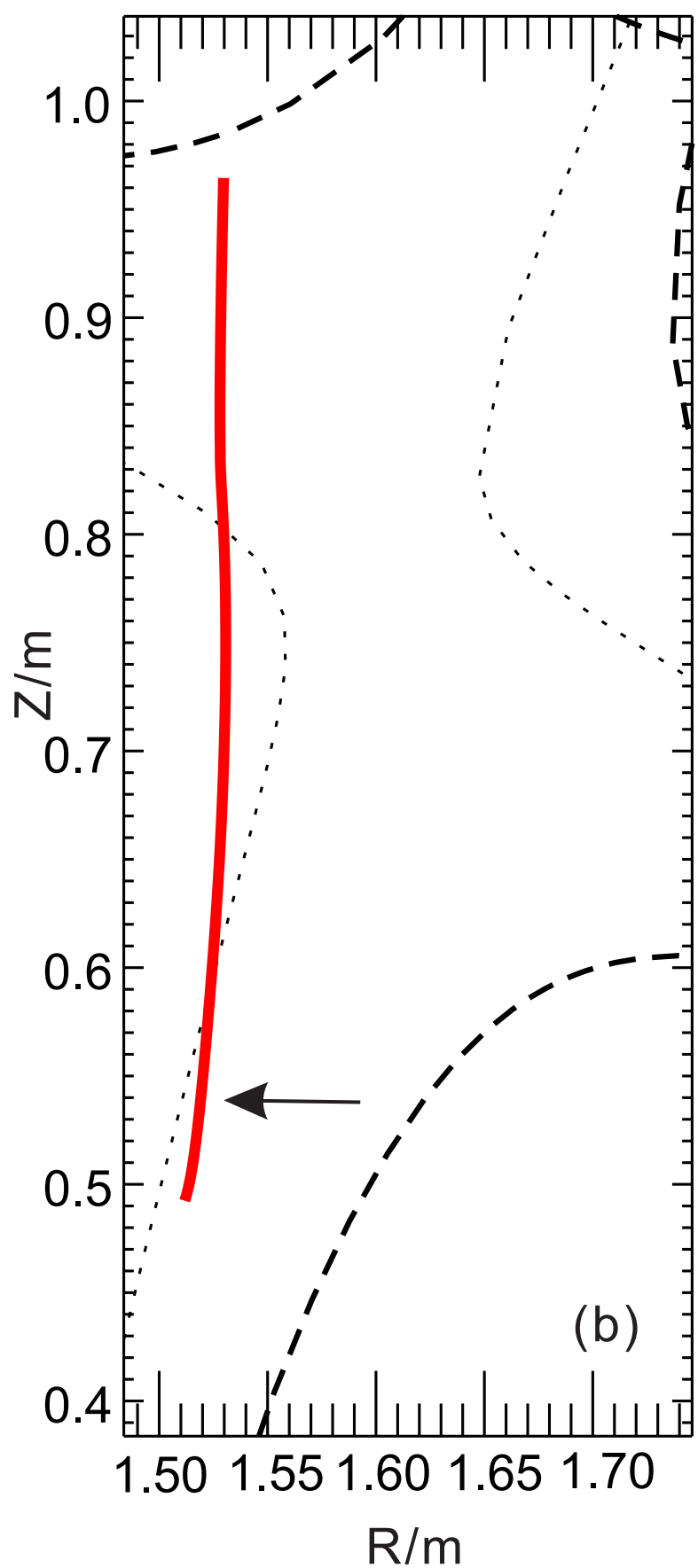
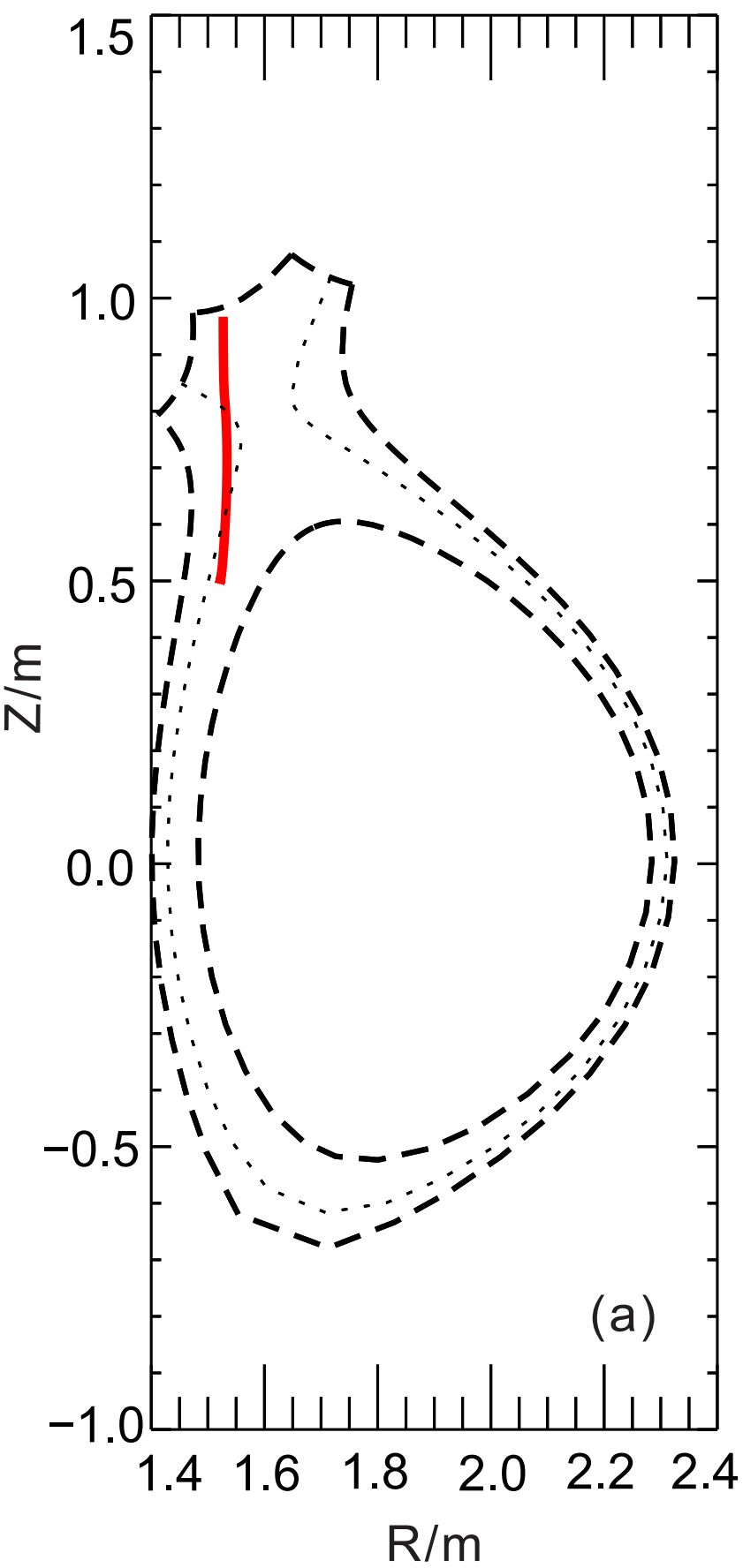
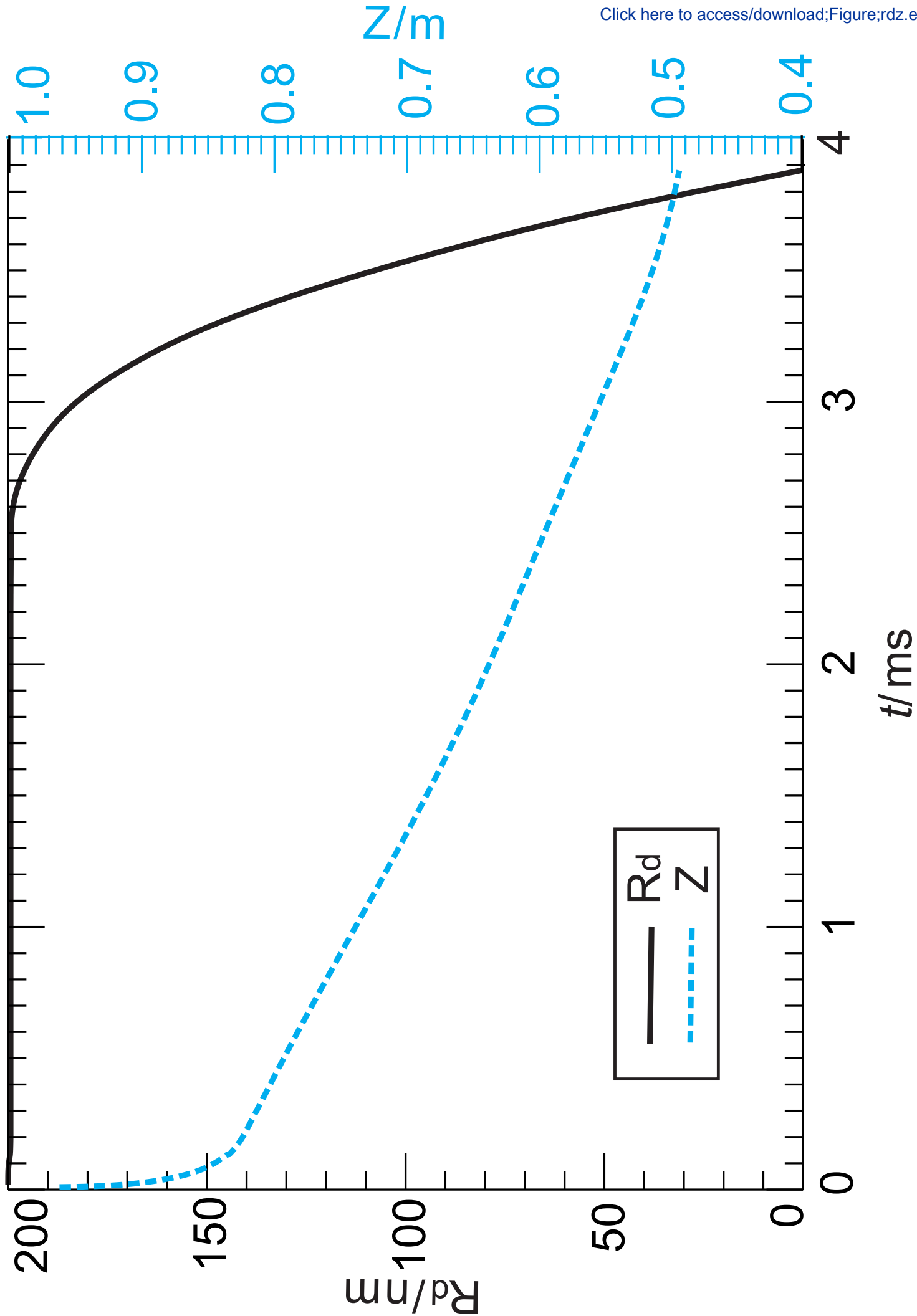
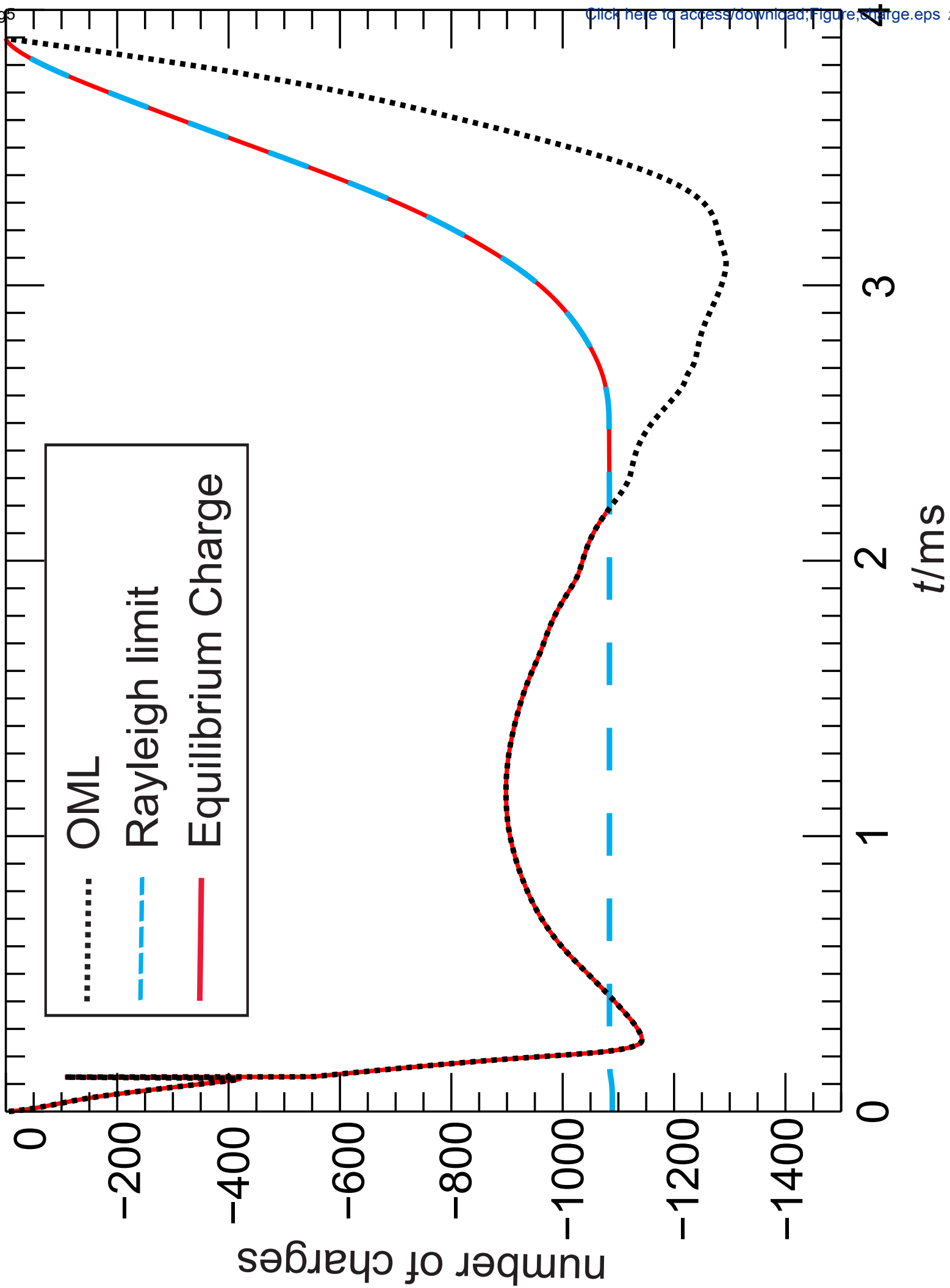
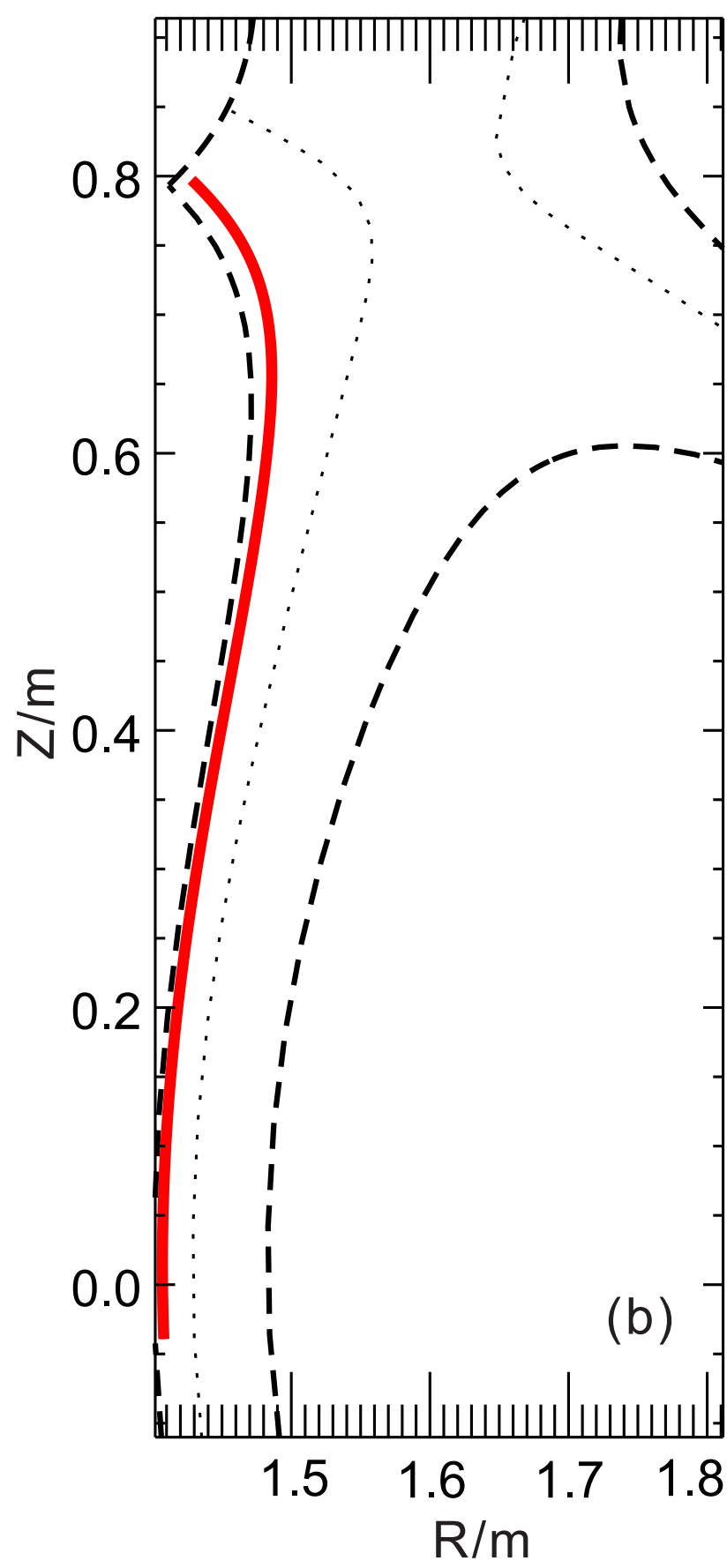
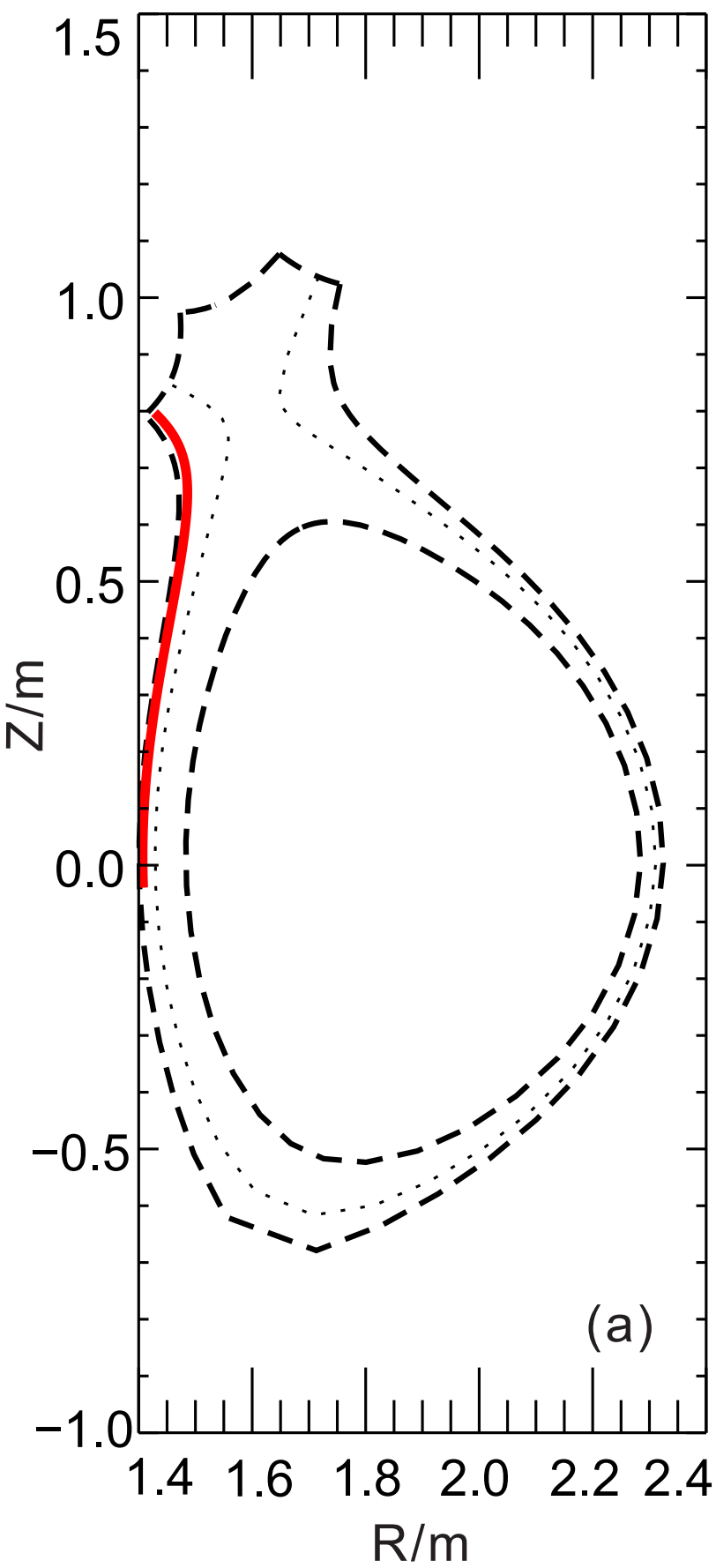
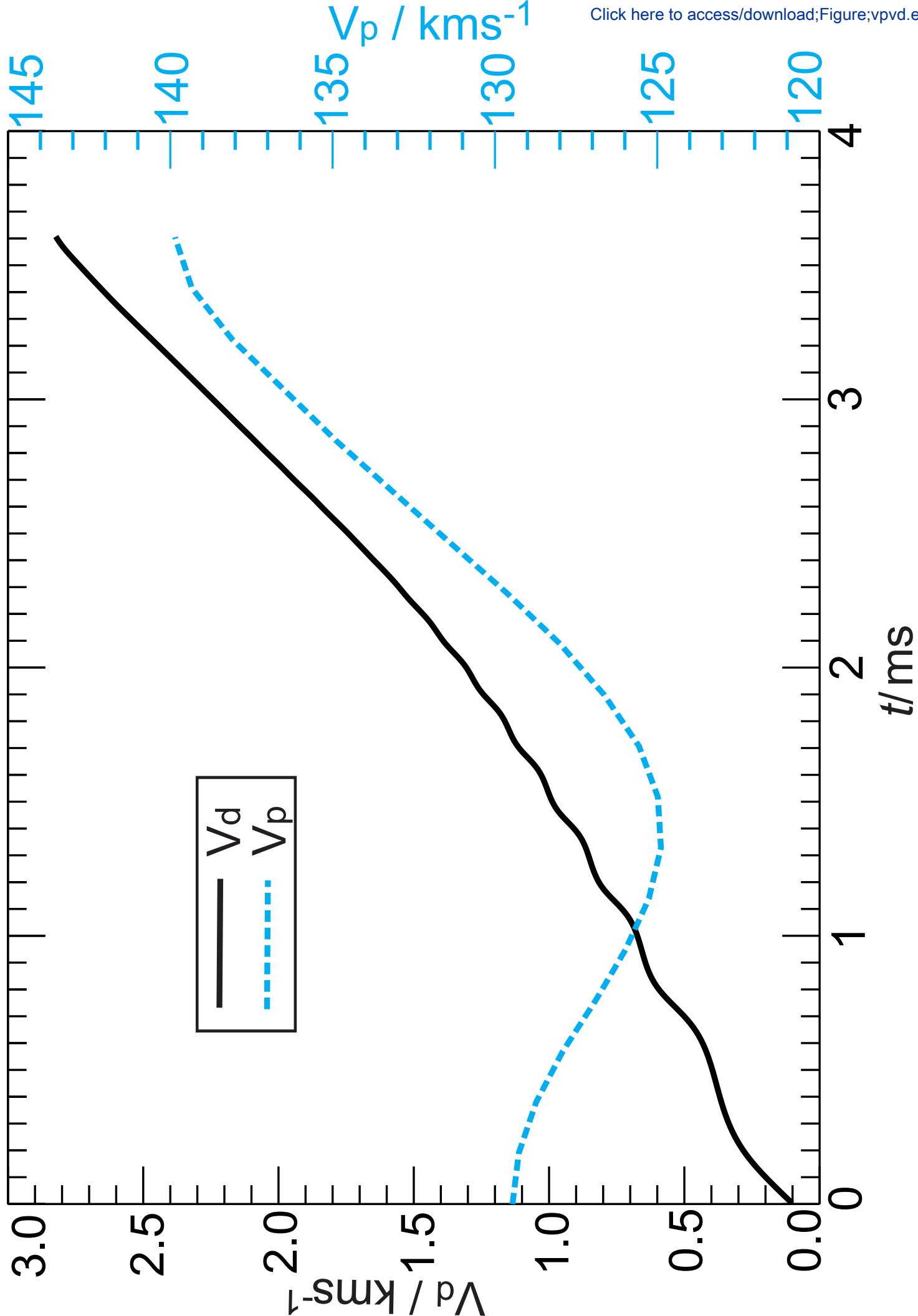


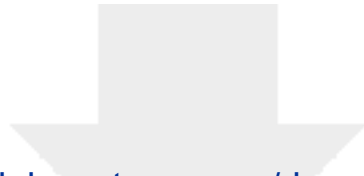
Fig4





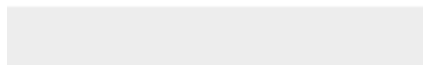






[Click here to access/download](#)

LaTeX Source File
Feng_EASTsim.tex



Declaration of interests

The authors declare that they have no known competing financial interests or personal relationships that could have appeared to influence the work reported in this paper.

The authors declare the following financial interests/personal relationships which may be considered as potential competing interests:

Roman Smirnov, rsmirnov@eng.ucsd.edu, UCSD, USA
Sergei Krasheninnikov, skrash@mae.ucsd.edu, UCSD, USA

These two scientists have conflicts with the first author.